Exploring The Radio Sky

Ambica Govind
Indian Institute of Technology Hyderabad

July 30, 2023

1 Towards Multiwavelength Astronomy

Before going into the specifics of radioastronomy it is imperative to understand the reason behind studying the sky in different wavelength regimes of the electromagnetic spectrum. The same object emits a spectrum of radiation whose intensity may be wavelength-dependent, in a way determined by its temperature and other internal mechanisms of radiation emission.
We begin by studying 2"X2" images of three radio-emitting galaxies from the CIRADA Image Cutout Server. The FITS Images were taken in different wavelength regimes by different galactic surveys: VLASS in radio(centre), WISE in infrared(right) and PanSTARRS in the Optical Regime(left).

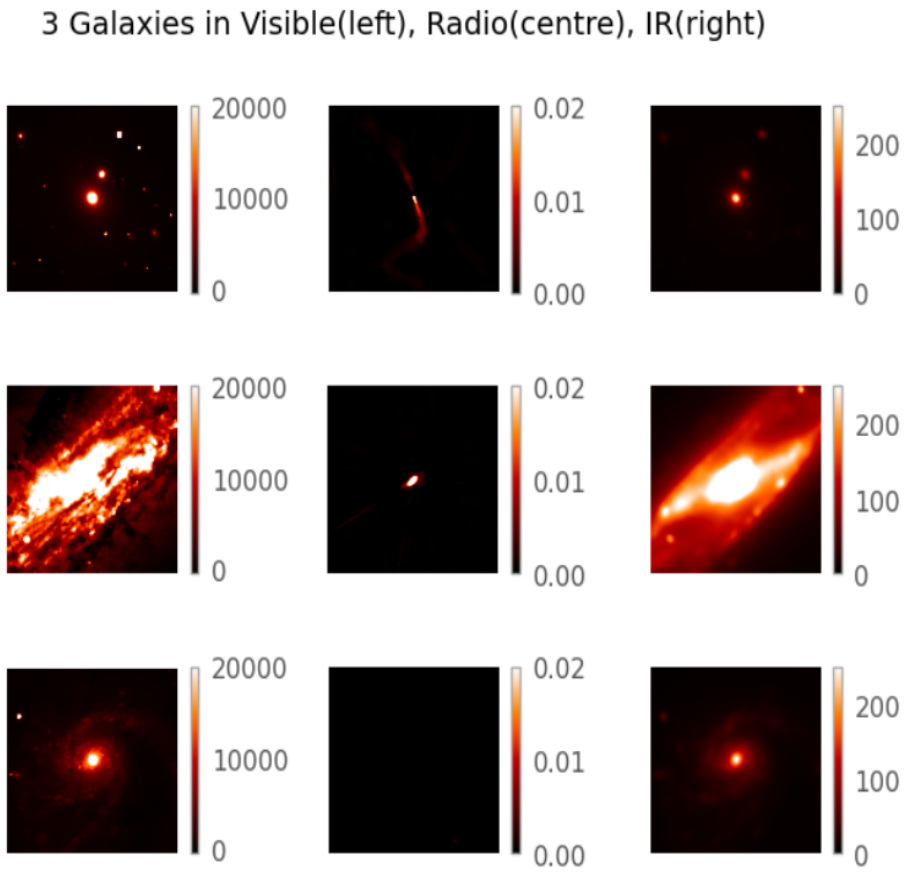

Figure 1: NGC 0383(top),NGC 0253(middle),MESSIER 099(bottom)

The infrared and optical bands render similar images of NGC 0383, however the VLASS Image shows jets of gas being thrown out in either directions of the galactic centre, suggesting the presence of a low-luminosity Active Galactic Nucleus. The jets are in many cases instances of synchrotron radiation. Blandford et al[1] explains that these are formed by intense magnetisation of the space

around the AGN, with the collimation facilitated by the magnetic stress associated with the accretion disk wind.

NGC 0253 shows high luminosity in the optical region and the infrared emission brings out the bright spiral bars indicating regions of active star formation. As before the radio image shows only the centre of the galaxy. It appears that supermassive black holes observed to be at the centre of most galaxies are strong sources of radio emission.
MESSIER 099 is a spiral galaxy; one can see spiral features in the optical and IR regions whereas the radio image does not show any feature.

Optical and IR images seem to be fairly similar since they are both driven by thermal processes. Radio emission however is driven by processes such as synchrotron emission. Radio being of longer wavelength is also quite penetrable to dust and matter on the galactic disc which enables us to 'see through' them directly into the galactic centre. It can be observed that different wavelengths give different aspects of insight on an astronomical object such as the physical processes that govern dynamics and evolution which underscores the importance of multiwavelength astronomy.

2 Towards Radioastronomy

In this section we do preliminary analyses of data available in the radio region of the spectrum

2.1 Jet Afterglow Lightcurve of GW170817

As a prelude to the upcoming analyses we plot the afterglow curve of the binary neutron star merger G170817 using a dataset compiled by Makhathini et al[2]. This is essentially a plot of the flux density of the signal against time since the merger event. The plot is corresponds to data from the VLA(Very Large Array)for the frequency 3 GHz. The peak observed is possibly the point at which the jet is directed straight at us.

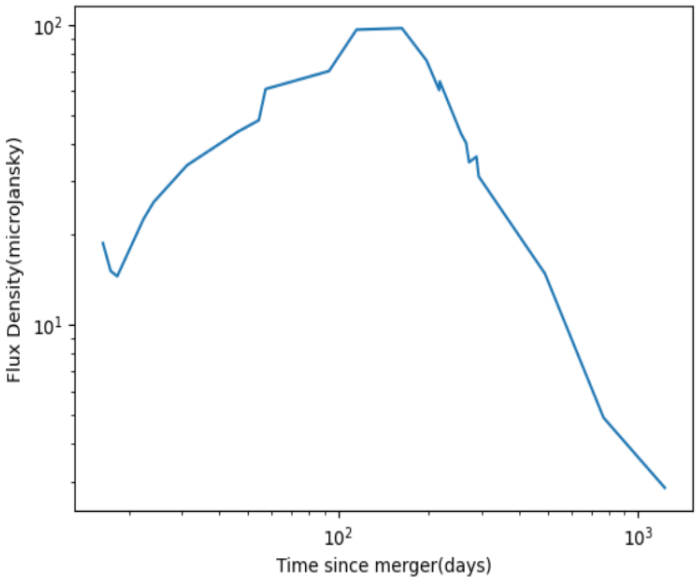

Figure 2: Jet Afterglow Curve of GW170817

2.2 Cosmic Microwave Background

As highlighted in the previous section, temperature happens to be a key feature that can be extracted by studying spectra of different radiative processes.
Here we look at the Cosmic Microwave Background, a relic of the Big Bang, and the nearest black body in nature known to us. The CMB is instrumental in improving our understanding of the primordial universe, and has been one of the most successful *a priori* predictions of the λCDM Model in Cosmology . It happens to glow the strongest in the microwave region of the radio spectrum.
We investigate far IR data adapted from the COBE Satellite[3] that provides us the Flux Density against the frequencies.

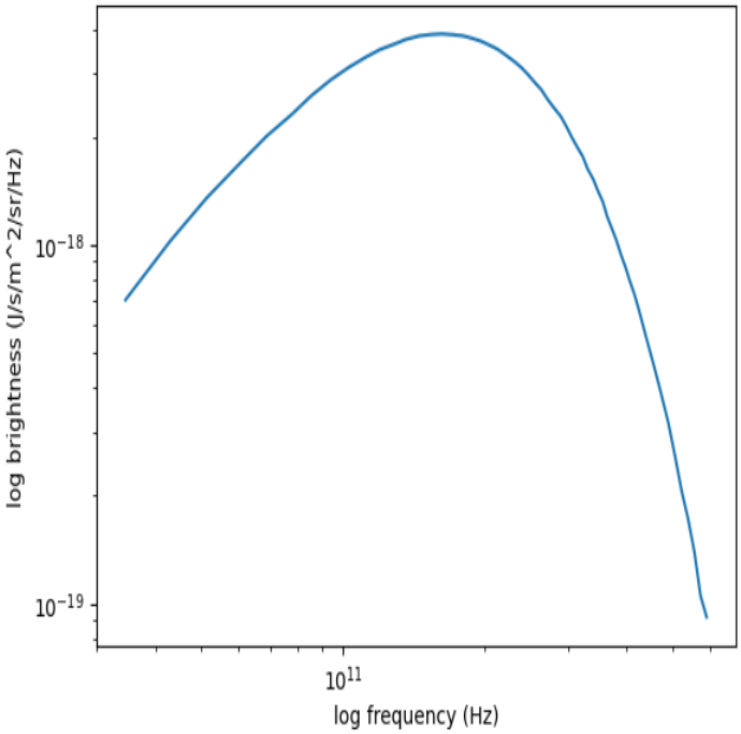

Figure 3: A log-scale Plot of spectral radiance against frequency

We use Planck's Law to estimate the temperature of the CMB:

$$B(\nu, T) = \frac{2h\nu^3}{c^2} \cdot \frac{1}{e^{\frac{h\nu}{kT}} - 1}$$

where $B(\nu, T)$ is the spectral radiance at a frequency ν and temperature T, $h = 6.634 \times 10^{-34} Js$ is Planck's Constant, $c = 3 \times 10^8 m/s$ is the speed of light and $k = 1.38 \times 10^{-23} J/K$ is Boltzmann's Constant.
We employ scipy to do elementary curve fitting and obtain a result of $2.738K$.

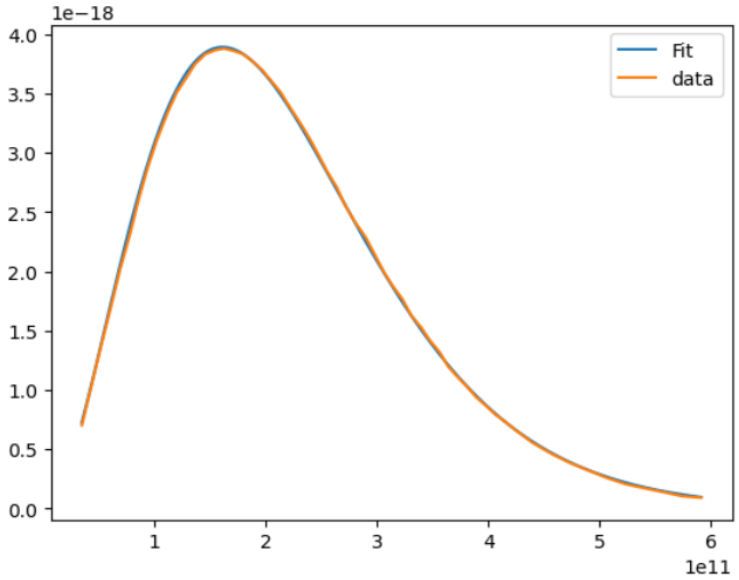

Figure 4: A linear-scale Plot of Brightness against frequency comparing the data and fit.

2.3 21-cm line Astronomy

Widely regarded the most important probe in the cosmos, the 21 cm spectral line is the result of a hyperfine transition in neutral hydrogen where an electron reverses its spin state to align/dis align with the nucleus. Its effect is small but measurable.
Quantum mechanics forbids this transition and thus it has an extremely low probability(once in 10 million years). Thus when one observes this spectral line its likely they are looking at something ancient, opening new avenues for cosmology research.
Here we present a simple application exploiting the 21-cm line to plot the galactic rotation curve of a distant edge-on galaxy using synthetic spectra. We fit a Gaussian to the spectral line and determine the central frequency and use the displacement from the expected value to find the doppler velocity.

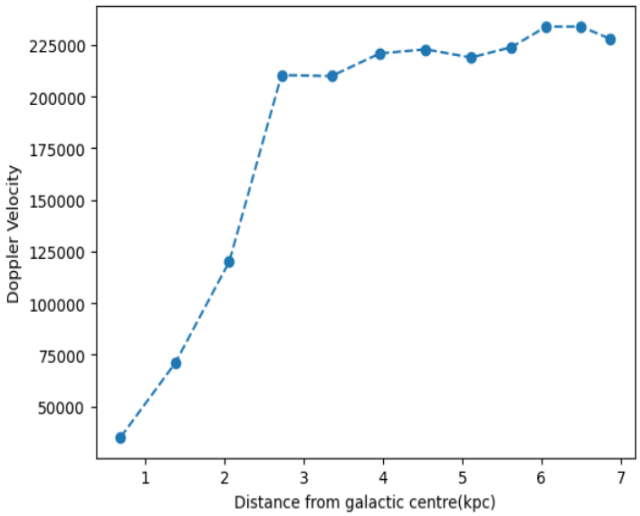

Figure 5: Galaxy Rotation Curve. The flatness is an anomaly to Newtonian Dynamics and hints the presence of a dark matter halo.

3 On Radioastronomy

3.1 Imaging In Radioastronomy

The starting point of a radioastronomer's work, imaging in radioastronomy is restricted in multiple engineering aspects including concerns of wavelength and complexity.
As an essential first step to make a map, we convolve the actual flux density distribution of the sky with the beam pattern characteristic to the telescope(a point spread function), to determine the antenna temperature, T_A, using

$$T_A(\theta_0, \phi_0) = \frac{A_{eff}}{2k} \int_{wholesky} I_\nu(\theta, \phi) P_{bm}(\theta - \theta_0, \phi - \phi_0) d\Omega$$

where $\frac{A_{eff}}{2k}$ is the Degrees per flux Density Unit, a conversion factor from Jy to K, the factor of 2 accounting for no detection in the other polarised component. This is what internally happens when the initial image is taken.
However the process of convolution can deprive the observer of resolution in the data, as the resolution is dictated by the FWHM of the main beam. Knowing the beam pattern, we deconvolve the beam from the observed data to get a better resolution.
A reliable deconvolution mandates a separation of data points no smaller than half the beam width(a spatial analog of Nyquist's Sampling Theorem). According to expectation the quality also increases with a high SNR.

Imaging in Aperture Synthesis
Aperture Synthesis employs the use of multiple dishes with a large spatial separation in order to increase the effective diameter of the telescope, hence improving resolution. It employs the technique of interferometry to form the image.
Visibility in the u-v plane is computationally calculated as the Discrete Fourier Transform of the intensity in the x-y plane, i.e. the plane of the source:

$$V(u, v) = \Sigma_x \Sigma_y I_\nu(x, y) e^{2\pi\iota(ux+vy)}$$

. Cells that contain no visibility data are skipped and so the Fourier transform effectively interpolates over these pixels and this leads to an imaging error. Yet another Fourier Transform gives the dirty beam. The interferometer as a whole has a beam pattern(a PSF) in this case; this synthesised beam pattern is determined by the combination of all the different baselines that go into making the image. The convolution of the dirty beam with this pattern gives the dirty image. We then deconvolve the beam pattern from the dirty image via the CLEAN Algorithm or its variants to obtain a usable astronomical image.

3.1.1 The CLEAN Algorithm

This is the algorithm used by CASA and many such softwares to deconvolve the dirty beam.
1. Determine the brightest pixel in the map and infer a fraction of the flux density to be the real emisssion(gain). Store the flux density and the location.
2. Convolve the clean component with the dirty beam centered on the location of the clean component and subtract from the map, yielding a residual map.
3. Repeat 1 and 2 until there is only random noise left.
4. Calculate a clean beam(a 2D elliptical Gaussian) by fitting a 2D Gaussian to the central lobe of the dirty beam.
5. Convolve all clean components with the clean beam and add back into the residual map.

3.2 CASA

CASA is NRAO's data processing software that provides tools for data reduction and imaging pipelines for both single-dish radiotelescopes and those working on aperture synthesis, such as VLA and ALMA.

3.2.1 Imaging TW Hydrae

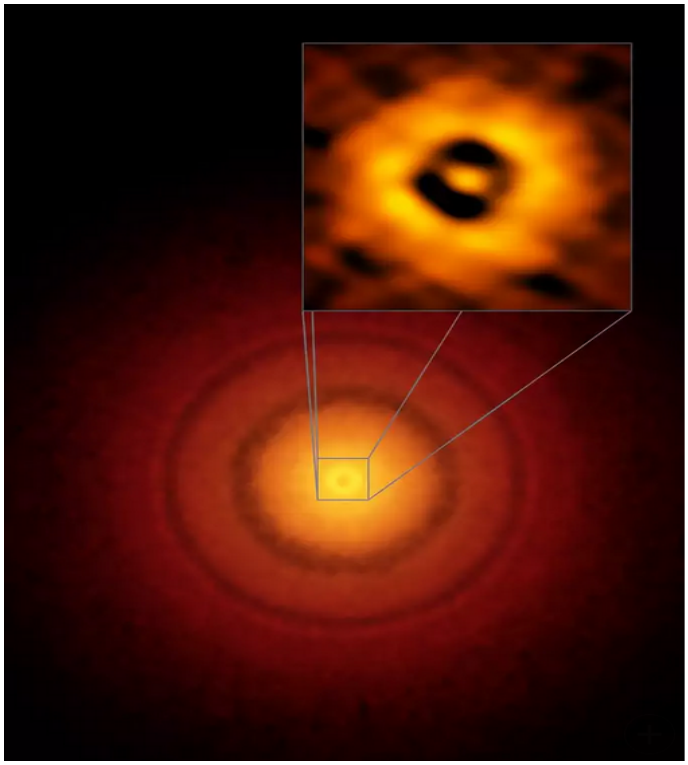

Figure 6: ALMA's image of TW Hydrae, young star in the constellation Hydra surrounded by a protoplanetary disk of gas and dust. At a distance of 176 light-years from Earth, this is one of the closest protoplanetary disks known.

The data comes from observations from 21 of the ALMA 12-m main array antennas and has been already calibrated. Part of it has been used in Qi et al 2013[4].
We load the measurement set into CASA, first plotting the visibility plane, showing the spatial frequencies detected from the source.

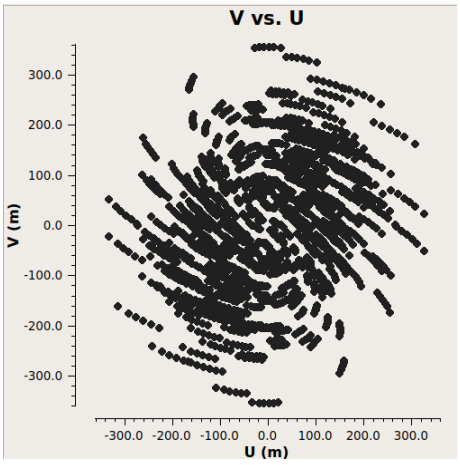

(a) U-V Plot of TW Hydrae

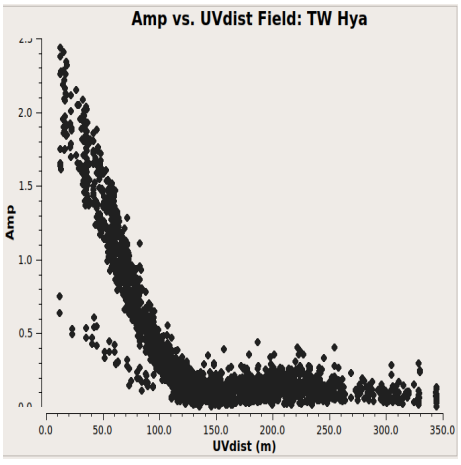

(b) Amplitude vs UVDist

The Point Spread Function, representative of the beam pattern of the ALMA Interferometer can be visualised thus in CASAviewer:

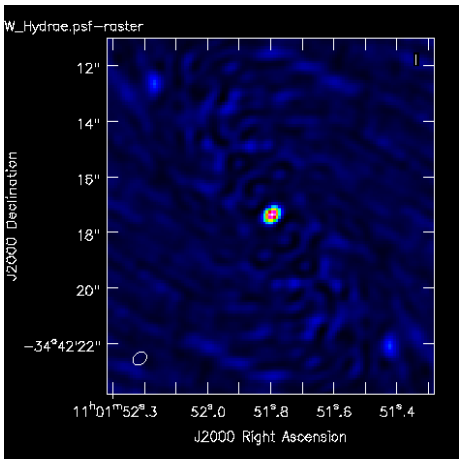

Figure 7: PSF of the beam pattern

We use tclean, the CASA Command that performs the CLEAN Algorithm(left) to deconvolve four times, leading to the final image of the protoplanetary disk(right).

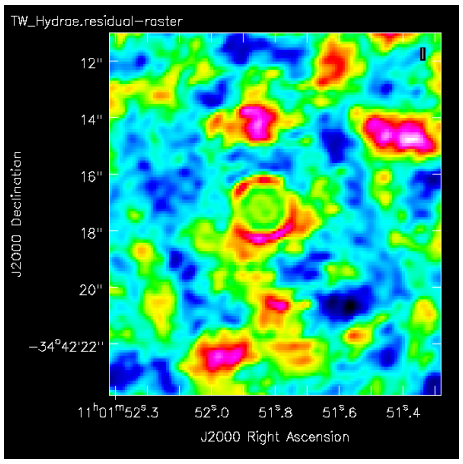

(a) Residual of TW Hydrae, after tclean

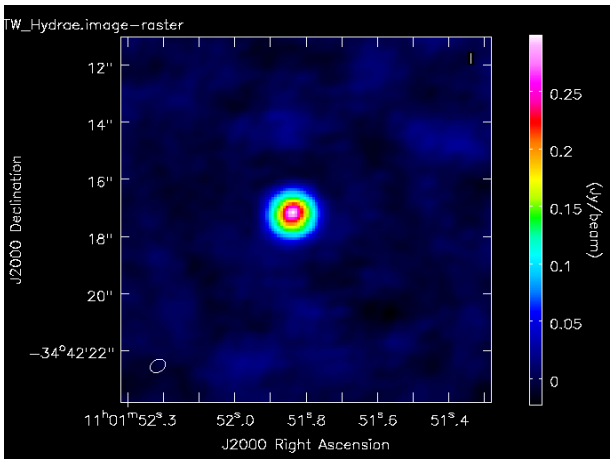

(b) Final image of TW Hydrae

Figure 8: Processing results in CASA

The imstat command in CASA gives an integrated flux density of about 1.512 Janskys in the region around the source.

3.2.2 Supernova Remnant 3C 391- An Extended Source

As before we visualise the UV Plot and calibrated visibility amplitude of the supernova remnant across the sky:

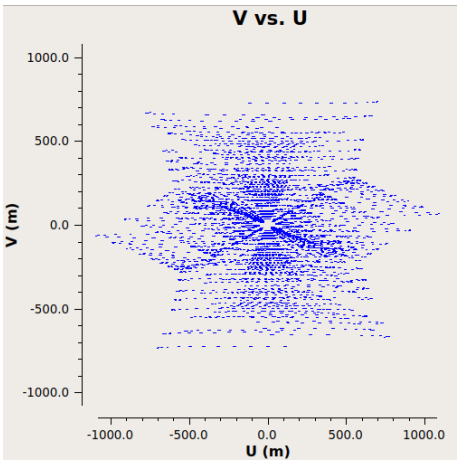

(a) U-V Plot of 3C 391

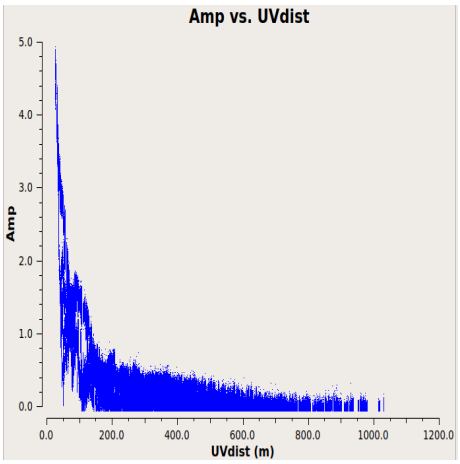

(b) Amplitude vs UVDist(baseline distance)

Note that the calibrated visibility amplitude bears semblance to a single-slit diffraction pattern hinting that the object of concern is an extended source.
Here we tweak the procedure a bit. Unlike last time we will use a multi-scale cleaning algorithm. The supernova remnant contains both diffuse, extended structure on a large and finer filamentary structure on smaller scales. The mosaic algorithm will do the best possible job in modelling the image.

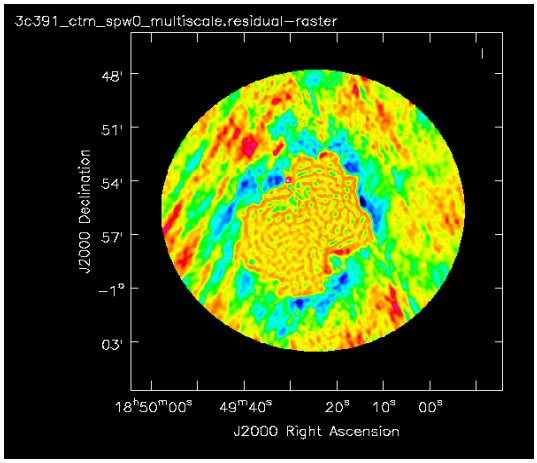

(c) Residual

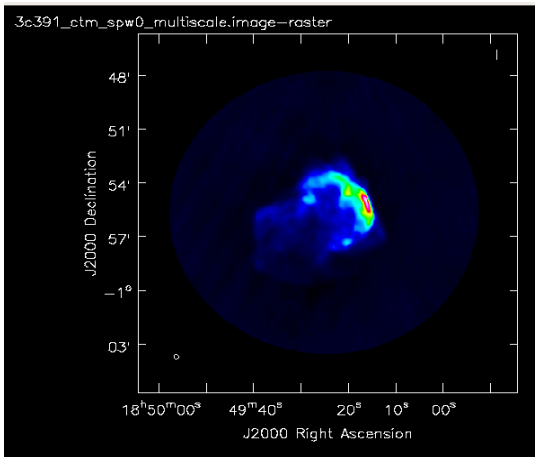

(d) Final Image of 3C-391

The integrated flux density is 7.79 Jy.

3.3 Model Fitting: Panchromatic Afterglow Lightcurve of GW170817

3.3.1 Markov Chain Monte Carlo Analysis

It is a technique for sampling from a probability distribution and using those samples to approximate desired quantity.
Markov Property: The probability of jumping from one state to the next state depends only on the current state and not on the sequence of previous states that lead to this current state.
This assumption saves a lot of computational time and happens to be realistic as well.
Bayes Theorem:

$$P(A|B)_{posterior} = \frac{P(B|A)_{likelihood} P(A)_{prior}}{P(B)_{normalisingconstant}}$$

Estimating the Posterior using Bayes can be difficult sometimes, as computing marginalized probability P(B) can be computationally expensive, especially when it is a continuous distribution.
To avoid the calculation altogether, we start with some random probability distribution and gradually move towards desired probability distribution.
The following cartoon succinctly summarises the essence of the algorithm, as the program tries to go closer to the destination:

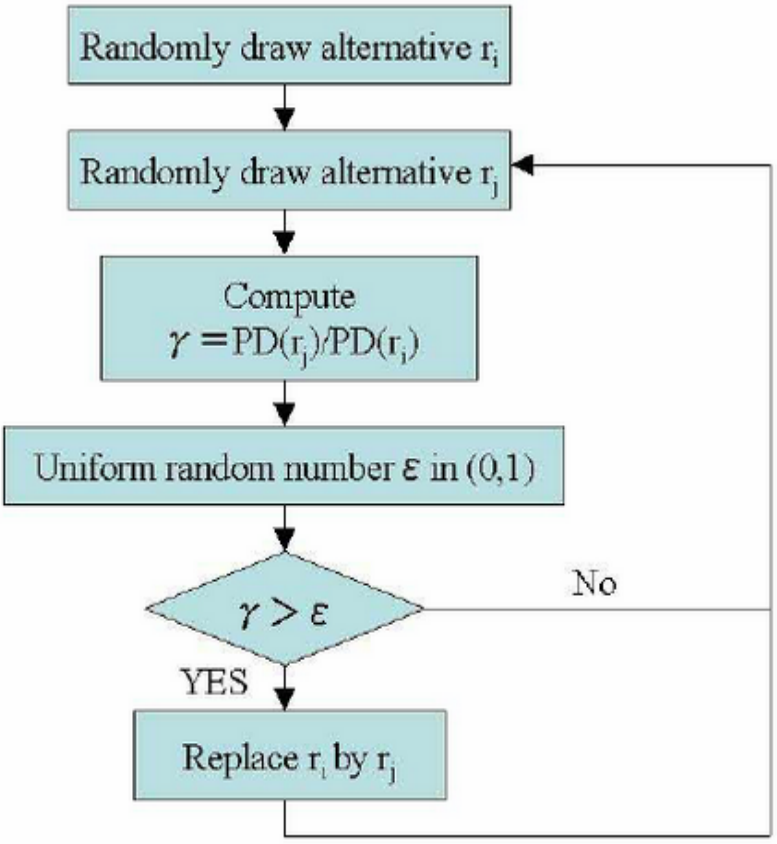

Figure 9: Graphical Explanation for MCMC

3.3.2 Fitting the model to data

The lightcurve of GW170817 has been well-modelled via numerical simulations as in Xie et al 2018[5], as a smooth broken power law:

$$F(t,\nu) = 2^{\frac{1}{s}} \left[\frac{\nu}{3GHz}\right]^{\beta} F_p \left[\frac{t}{t_p}^{-s\alpha_1} + \frac{t}{t_p}^{-s\alpha_2}\right]^{-\frac{1}{s}}$$

where ν is the observing frequency, β is the spectral index, F_p is the flux density at the $3GHz$ lightcurve peak, t is the time post-merger, t_p is the lightcurve peak time, s is the smoothness parameter and α_1 and α_2 are the power law rise and decay slopes respectively.

Sticking to the same dataset as in 2.1, we now consider data from VLA as well as Chandra for our further analysis.

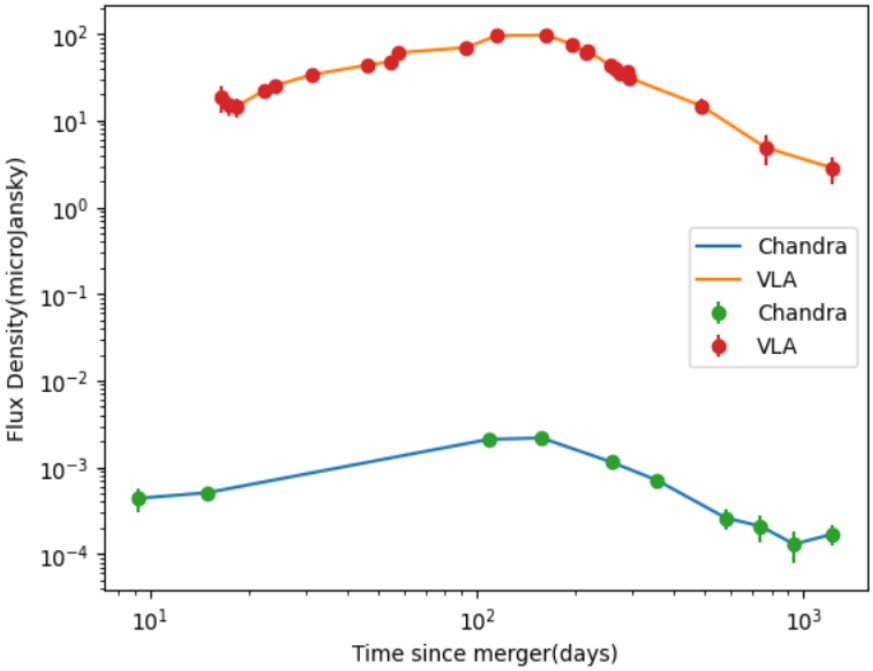

Figure 10: GW170817 Afterglow Lightcurves

We use the emcee package in Python to perform a Markov-Chain-Monte-Carlo Analysis and fit the model to the VLA 3GHz data and Chndra data of frequency $2.41 \times 10^{17} Hz$(same as in 2.1) with 100 walkers, 1000 steps and flat priors and obtain a good fit. The results and plots are summarised below.

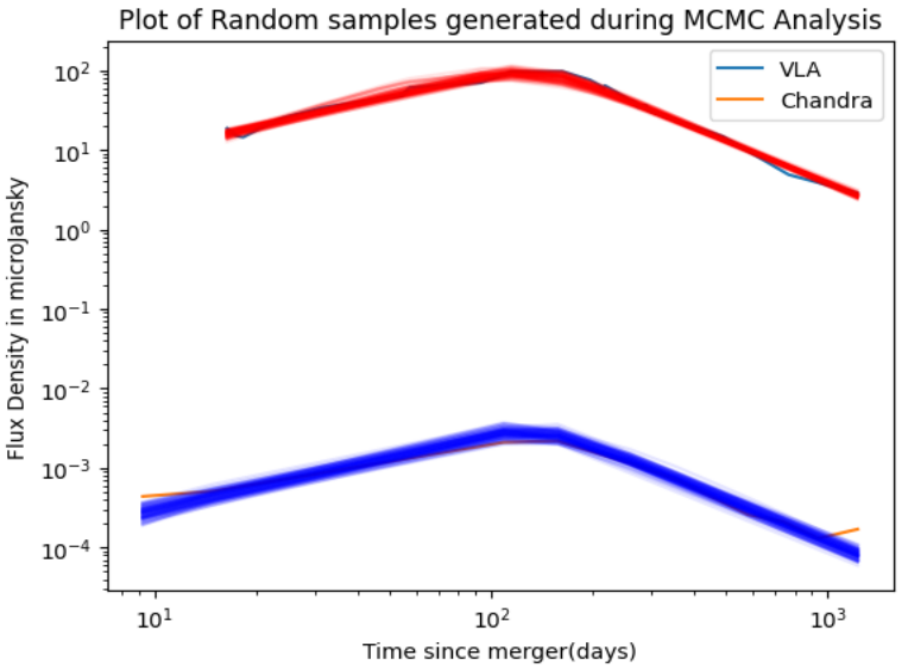

(a) Fit generated by a random bunch of samples from VLA (3GHz) data

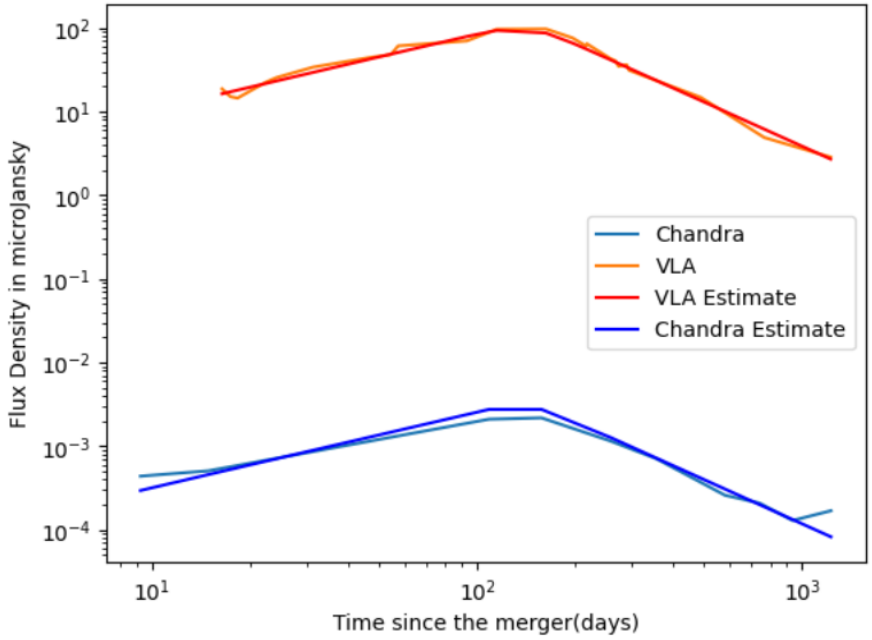

(b) Comparison of observations against the fit

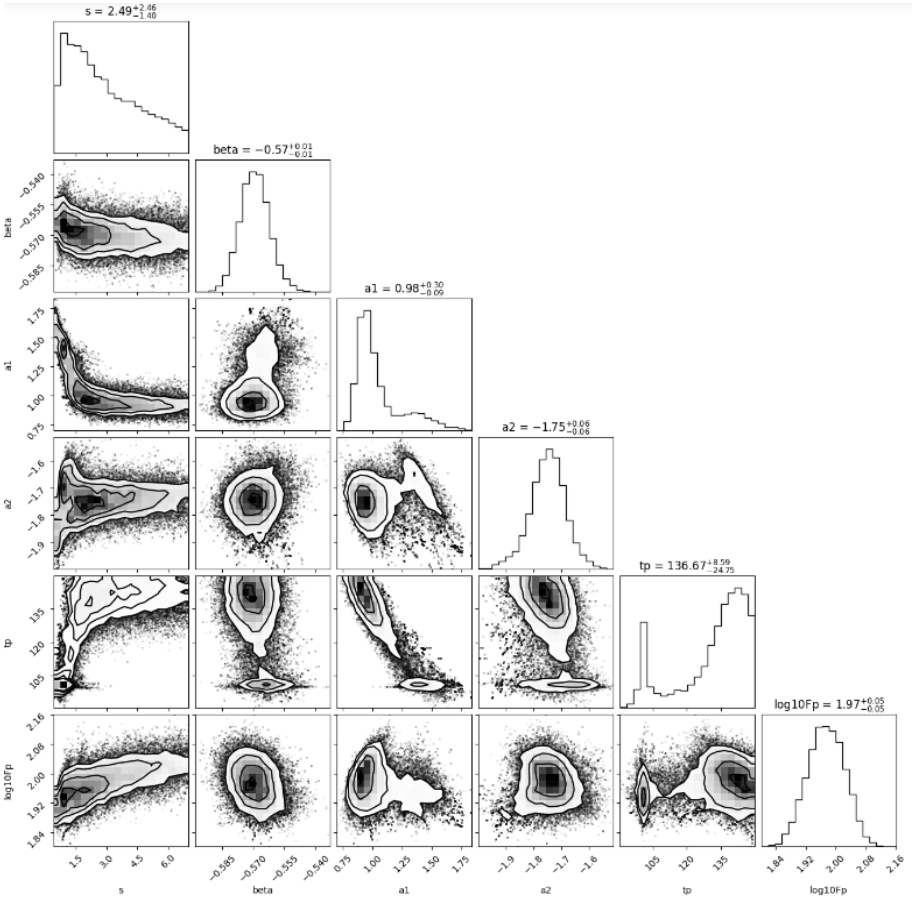

Figure 11: Posterior Distributions

Note that the corner plot doesn't look as good as desired, owing to the fact that only two frequencies have been used. However its still quite informative, in that it conveys information about the parameters used in the power law.

3.4 Fast Radio Bursts

3.4.1 Introduction

A fast radio burst (FRB) is a transient radio pulse of length ranging from a fraction of a millisecond to 3 seconds. They are produced by high energy astrophysical processes that are not yet understood completely. Most of the sources emitting FRBs are known to be extragalactic, while some of them do originate in the Milky Way. They come in repeating as well as non-repeating signals.
There is no general consensus within the scientific community w.r.t the origin of FRBs. Suggestions include compact object mergers and magnetars. A host of scientific groups such as the CHIME Collaboration actively look for FRBs and study them, looking to pinpoint their sources and study their properties.

3.4.2 Dispersion Measure

To a certain extent, telescopes and surveys are capable of estimating the distance to astronomical sources(note that this is harder for ground-based telescopes) using the parallax method, or using Cepheid Variables/RR Lyrae Stars.
But beyond a certain limit, it becomes difficult to maintain accuracy in distance measurement and we are forced to resort to estimating cosmic distances by using other quantities as a proxy. One such quantity is the dispersion measure.
The technical definition is: "integrated column density of free electrons between an observer and a pulsar".
Physical manifestation: Electromagnetic Radiation is slowed down by the matter they pass through. Longer the wavelength, the more it is slowed. Dispersion measure is a measure of how much delay results from additional wavelength, which is bound to increase with distance to the source.
The arrival time of each frequency component of the signal is obtained from observations. It is quantified by the following equation:

$t_{arr} \propto \frac{DM}{\nu^2}$ (1)

Ths constant for proportionality is found to be 4.14880810^3 where t_{arr} is in s, ν is in MHz and is in $pccm^3$.

3.4.3 DM of B0011+47

Here we try to compute the DM of a pulsar, B0011+47. The data consists of intensities for a time range comparable to the pulse duration for a frequency spectrum ranging 400-800MHz. The blip can be visualised as a spectrogram below(observe that the lower frequencies arrive after the higher ones):

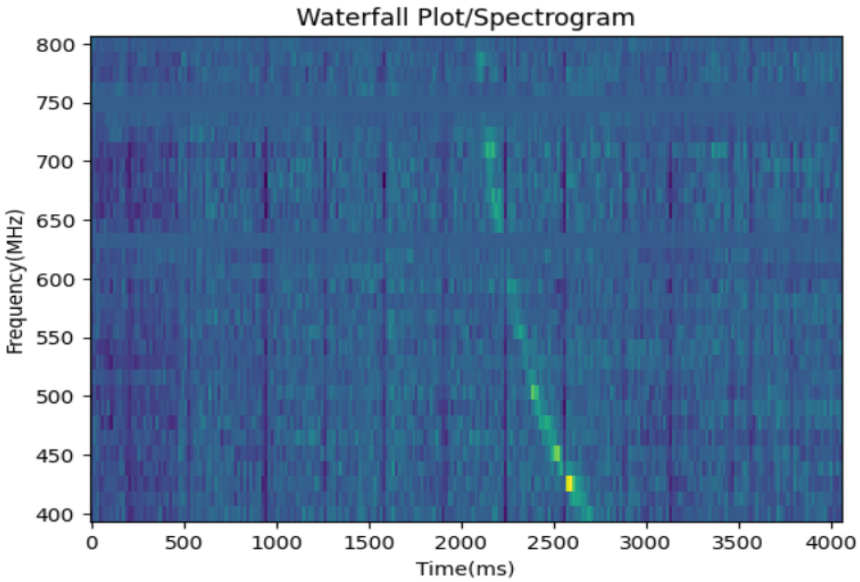

Figure 12: Waterfall Plot of Pulsar Data

We then employ Eq (1) to calculate the delay in arrival time for different frequencies corresponding to Dispersion Measures ranging from typical values of 1-1000.
Our aim is to line up the pulse in all frequencies at the same instant of time, by shifting the data leftwards by an amount that corresponds to the delay caused by dispersion. For the given range of DMs, the best plot(closest to a vertical line) will be obtained for the best estimate of the dispersion measure.
To quantify the closeness of these DMs to the 'correct DM', we calculate the Time-series corresponding to each DM by adding up intensities in all frequencies. We further define the SNR(Signal-to-Noise Ratio) as the ratio of the maximum of the absolute value of the time series to the mean of the absolute value of the time series.
We calculate these SNRs and find the DM where SNR is maximum. This de-disperses the data and the best DM gives a distinct peak in Time Series.

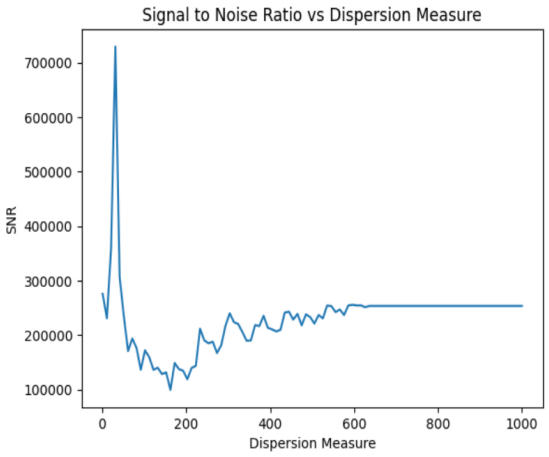

(a) Residual

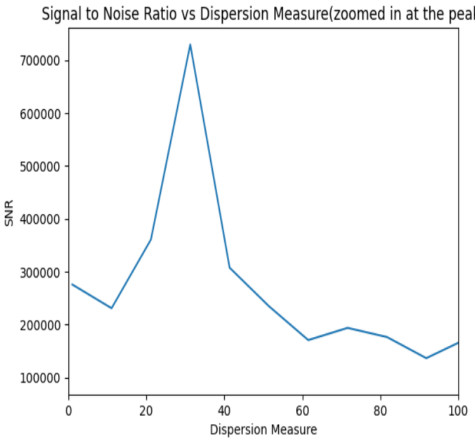

(b) Final Image of 3C-391

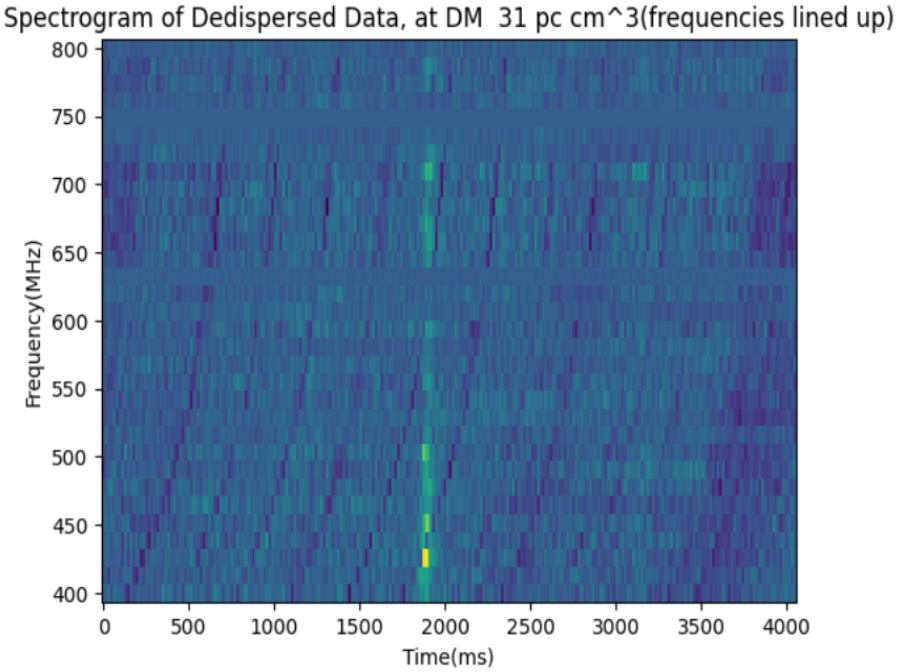

4 Conclusion

What follows is the gist of the project compressed into a few bullets:

1. It is desirable to study the sky in different wavelengths, since every wavelength has different mechanisms of emission. This is done so we may not miss out on sources. Radio is an effective way to look deep into structures because they are least scattered by the interstellar medium.

2. Common radio sources are galactic centres containing supermassive black holes, supernova remnants, pulsars(rotating neutron stars with high magnetic fields), the CMB and Fast Radio Bursts.

3. The 21-cm line of the spectrum of neutral hydrogen arising from quantum transitions is one of the most important probes to study the primordial universe. It happens to occur in the radio-region of the spectrum.

4. In the tasks performed in this project, we conclude that image processing and analysis, fitting models to data and basic signal processing are key to scientific research in radioastrophysics. Software like CASA and basic Python libraries help us achieve this to do the necessary science.

References

[1] R. Blandford, D. Meier, and A. Readhead, "Relativistic jets from active galactic nuclei," *Annual Review of Astronomy and Astrophysics*, vol. 57, pp. 467–509, 2019.

[2] S. Makhathini, K. P. Mooley, M. Brightman, K. Hotokezaka, A. Nayana, H. T. Intema, D. Dobie, E. Lenc, D. A. Perley, C. Fremling, *et al.*, "The panchromatic afterglow of gw170817: the full uniform data set, modeling, comparison with previous results, and implications," *The Astrophysical Journal*, vol. 922, no. 2, p. 154, 2021.

[3] J. C. Mather, E. Cheng, R. Eplee Jr, R. Isaacman, S. Meyer, R. Shafer, R. Weiss, E. Wright, C. Bennett, N. Boggess, *et al.*, "A preliminary measurement of the cosmic microwave background spectrum by the cosmic background explorer (cobe) satellite," *Astrophysical Journal, Part 2-Letters (ISSN 0004-637X), vol. 354, May 10, 1990, p. L37-L40.*, vol. 354, pp. L37–L40, 1990.

[4] C. Qi, K. I. Öberg, D. J. Wilner, P. d'Alessio, E. Bergin, S. M. Andrews, G. A. Blake, M. R. Hogerheijde, and E. F. Van Dishoeck, "Imaging of the co snow line in a solar nebula analog," *Science*, vol. 341, no. 6146, pp. 630–632, 2013.

[5] X. Xie, J. Zrake, and A. MacFadyen, "Numerical simulations of the jet dynamics and synchrotron radiation of binary neutron star merger event gw170817/grb 170817a," *The Astrophysical Journal*, vol. 863, no. 1, p. 58, 2018.